

# Fabrication of Polymeric Nanorods Using Bilayer Nanoimprint Lithography\*\*

Fatih Buyukserin, Mukti Aryal, Jinming Gao, and Wenchuang Hu\*

Polymeric nanoparticles are becoming increasingly important in a variety of biological applications, such as biomolecular sensing, diagnostic imaging, and therapeutic drug delivery.<sup>[1,2]</sup> For these applications, the mass production of multifunctional nanocomposite materials with precise control of particle size, shape, and composition is a significant challenge.<sup>[3,4]</sup> For instance, the use of conventional bottom-up strategies (e.g., emulsion polymerization) to fabricate polymeric nanostructures with nonspherical geometry and a uniform size distribution is difficult because these methods are typically driven by the minimization of interfacial free energy that yields spherical particles with a size variation.<sup>[3]</sup> Moreover, the formation of nanocomposite materials is difficult due to the challenge in assembling multiple components from large volume fractions of solvent. On the other hand, in the field of microelectronics, polymers as resist can be precisely patterned to have arbitrary shapes using state-of-the-art photo-, e-beam, and X-ray lithographic technologies.<sup>[5]</sup> They are limited either by high cost, poor accessibility, slow speed, or radiation damage to functional polymers. In the past decade, many low-cost nanopatterning techniques have been invented to pattern polymer structures, such as nanoimprint lithography (NIL)<sup>[6,7]</sup> and soft lithography,<sup>[8]</sup> among many others.<sup>[9–15]</sup> These methods are capable of making nanostructures of desired shape and size. However, it is not straightforward to produce large quantities of biofunctional nanoparticles using them. Most of these nanopatterning approaches, either imprinting or soft lithography, result in a residual layer that connects the periodic structures on a surface. Furthermore, they are limited

by the lack of large-scale nanopatterned molds for mass production and a reliable method to transfer particles from surface to solution.

Recently, several top-down engineering methods for producing size-controlled, nonspherical polymeric particles have been reported. These techniques involve the use of photolithography,<sup>[16,17]</sup> microfluidics,<sup>[18,19]</sup> soft lithography on non-wetting surfaces (PRINT),<sup>[20]</sup> step-and-flash imprint lithography (S-FIL),<sup>[21]</sup> and stretching of spherical particles.<sup>[4,22,23]</sup> Although these methods demonstrated different degrees of success, they also showed certain limitations in particle-size control, cost, and throughput. For example, the throughputs of the photolithography and microfluidic approaches are relatively low at this stage and the particle sizes are above 5  $\mu\text{m}$ .<sup>[16–19]</sup> The stretching method requires prefabrication of uniform spherical particles to maintain size uniformity,<sup>[4]</sup> and the PRINT and S-FIL methods require liquid precursors and costly nanopatterned molds.<sup>[20,21,24]</sup>

In this Communication, we report a bilayer nanoimprint lithography (B-NIL) method with large-scale, low-cost Si molds of high-density nanopores transferred from anodic alumina for the fabrication of free-standing polymeric nanorods with tunable lengths from 100 nm to 1  $\mu\text{m}$ . A sacrificial polymer layer is introduced to the imprinting procedure to form free-standing nanoparticles with the functional polymer. Large-scale Si molds with high densities ( $10^{10} \text{ cm}^{-2}$ ) and ordered arrays of nanopores are fabricated by plasma etching using anodic alumina membranes as a mask, which enables the fabrication of large quantities of nanorods ( $>10^{10}$  per imprint cycle) using nanoimprints on bilayer polymers. The same mold can be reused to prepare particles with different lengths by controlling the initial polymer thickness. Fluorescent nanoparticles are also fabricated by incorporating a dye molecule into the polymer matrix.

In a typical procedure, a nanoporous silicon mold is first prepared by inductively coupled plasma (ICP) etching with  $\text{Cl}_2/\text{Ar}$  gases using an anodized alumina membrane (AAM)<sup>[25]</sup> as an etch mask (Figure 1a). The Si mold is then modified with a fluorocarbon-based silane to form a self-assembled monolayer (F-SAM) for ease of demolding. As a proof of principle, a bilayer polymer substrate is prepared in which Si or quartz is spin coated first with a sacrificial poly(methyl methacrylate) (PMMA) layer and then a UV-curable SU-8 polymer layer. SU-8 is used in this study as a model polymer system because it is widely used in microelectronic mechanical systems for biomedical applications (Bio-MEMs)<sup>[26,27]</sup> and also because it

[\*] Prof. W. Hu, Dr. F. Buyukserin, M. Aryal  
Department of Electrical Engineering  
University of Texas at Dallas  
Richardson, TX 75080 (USA)  
E-mail: walter.hu@utdallas.edu

Prof. J. Gao  
Department of Pharmacology  
Simmons Comprehensive Cancer Center  
University of Texas Southwestern Medical Center  
Dallas, TX 75390 (USA)

[\*\*] This research is supported by the Montcrief Foundation. We thank C. Kessinger for assistance with confocal laser scanning microscopy and E. Kildebeck for helpful discussions.

Supporting Information for this article is available online under <http://www.small-journal.com> or from the author.

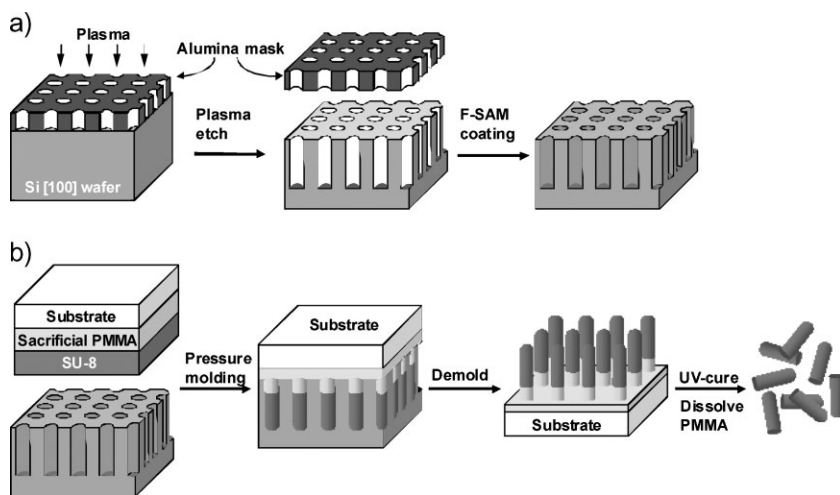


**Figure 1.** Fabrication of polymeric nanorods by bilayer nanoimprint lithography (B-NIL). a) Fabrication of nanoporous Si mold through plasma etching and surface treatment with fluorocarbons. b) B-NIL protocol for polymer imprinting and subsequent nanorod release.

makes it possible to incorporate various other materials (e.g., hydrophobic contrast agents). Imprinting is carried out by compressing the nanoporous Si mold onto the bilayer substrate under elevated pressure and temperature. Two different temperatures are used sequentially in the imprint process to eliminate the residual SU-8 layer. First, the SU-8 functional-polymer layer is imprinted at a temperature higher than the glass-transition temperature of SU-8 ( $T_g = 55^\circ\text{C}$ )<sup>[28]</sup> but lower than the  $T_g$  of PMMA so that only SU-8 will flow into the Si nanopores. Then, the temperature is raised significantly above the  $T_g$  of PMMA ( $T_g = 105^\circ\text{C}$ )<sup>[29]</sup> to allow PMMA to fill the rest of Si nanopores, thus resulting in SU-8 pillars separated by the sacrificial PMMA. After imprinting, the system is cooled down and the Si mold is released from the imprinted SU-8 nanopillars on the substrate. Free-standing SU-8 nanorods are then obtained after UV curing and dissolution of the sacrificial PMMA layer (Figure 1b).

As we have discussed earlier, the practical application of NIL for the mass production of nanoparticles is limited by the high cost and lengthy time requirement for making nano-patterned molds by conventional e-beam lithography. To address this challenge, we have utilized the self-assembled AAM as a mask to etch into Si to produce low-cost and large-area molds with high-density nanopores (Figure 1a). Previously, anodic aluminum oxide has been used as a mask for deposition or etching to transfer the nanostructures into other materials for various applications.<sup>[30–34]</sup> A similar process is optimized to obtain a large-area anodic alumina membrane, which is used as a mask to etch Si molds for the B-NIL process. Figure 2a shows the AAM produced by a two-step anodization method<sup>[25]</sup> on the underlying Al ( $\approx 50\text{ cm}^2$  on each surface of Al). Each AAM had two sides: the solution side in contact with the electrolyte during anodization, and the rough barrier side facing the Al.<sup>[35]</sup> Coupon-sized AAM masks (Figure 2a) can be harvested by a voltage reduction protocol<sup>[36]</sup> followed by physical detachment.

To produce the nanoporous Si mold, an AAM mask was placed on a Si[100] wafer (barrier side facing up) and ICP

etching was used to form the porous structures. Initially, it was necessary to remove the branches on the AAM using Ar plasma (10 mTorr, 10 min), producing a flat mask with uniform depth (Figure 2b). Then, a second etching procedure with a 1:1 mixture of Ar and  $\text{Cl}_2$  yields high-density, ordered arrays of nanopores on the Si surface (Figure 2c). Successful pattern transfer was confirmed by comparing the pore diameter and density of the AAM ( $97.6 \pm 1.0\text{ nm}$ ,  $7.0 \times 10^9\text{ pores cm}^{-2}$ ) to that of the Si mold ( $97.8 \pm 1.5\text{ nm}$ ,  $7.0 \times 10^9\text{ pores cm}^{-2}$ ). This nanoporous Si wafer was rendered nonadhesive by a fluorocarbon silane modification and used as a mold for the B-NIL studies.

Large arrays of polymer nanopillars were formed by imprinting the nanoporous Si mold on a polymer-coated Si or quartz substrate at elevated temperatures under

pressure. In a representative procedure, the substrate was first spin coated with a sacrificial PMMA layer (170 nm) and then with a SU-8 layer (200 nm). The pressure was first raised to 40 bar, and then the temperature was increased to  $100^\circ\text{C}$  to induce SU-8 flow into the pores, followed by a temperature increase to  $170^\circ\text{C}$  for PMMA flow. Figure 3a shows uniform and densely packed nanopillars ( $\approx 10^{10}\text{ pillars cm}^{-2}$ ) after the Si mold was released and the SU-8 pillars were cured with UV light ( $\lambda_{\text{max}} = 365\text{ nm}$ , 30–60 s). Similar results were observed for substrates with thinner SU-8 coatings (e.g., 65 or 100 nm) while the residual PMMA layer became thinner as a result of more PMMA flowing into the nanopores (see Supporting Information, Figure S1). In comparison, in the absence of a PMMA layer, nanopillars with variable lengths and void areas were seen on the substrate (Figure 3b). This result was observed for all the single-layer substrates with SU-8 thickness  $\leq 200\text{ nm}$ . We believe that this is a result of sample de-wetting, where polymer redistribution in such thin coatings caused local depletion zones during nanoimprinting.<sup>[37,38]</sup> In the bilayer setup, the use of a PMMA layer with a lower surface energy compared to Si effectively prohibits the onset of SU-8 dewetting and yields uniform polymer flow over large areas. Due to the poor contrast of PMMA and SU-8 under scanning electron microscopy (SEM), we could not detect their interface in the pillars. However, the PMMA flow into the mold is confirmed by the volume reduction in the PMMA layer (see details in Supporting Information, Figure S1). The volume of the SU-8 film is designed to be smaller than the mold cavity to ensure PMMA flow into the mold.

After particle formation and mold release from the substrate, SU-8 nanopillars were cured by UV exposure and then harvested by immersing the imprinted substrates in acetone to dissolve the PMMA layer. We found that the formation of free-standing nanorods without the SU-8 residual layer depended on the initial SU-8 coating thickness or volume relative to the mold depth or volume. Figure 4a shows transmission electron microscopy (TEM) images of the SU-8 nanorods that were joined by a thin residual layer of  $\approx 30\text{ nm}$

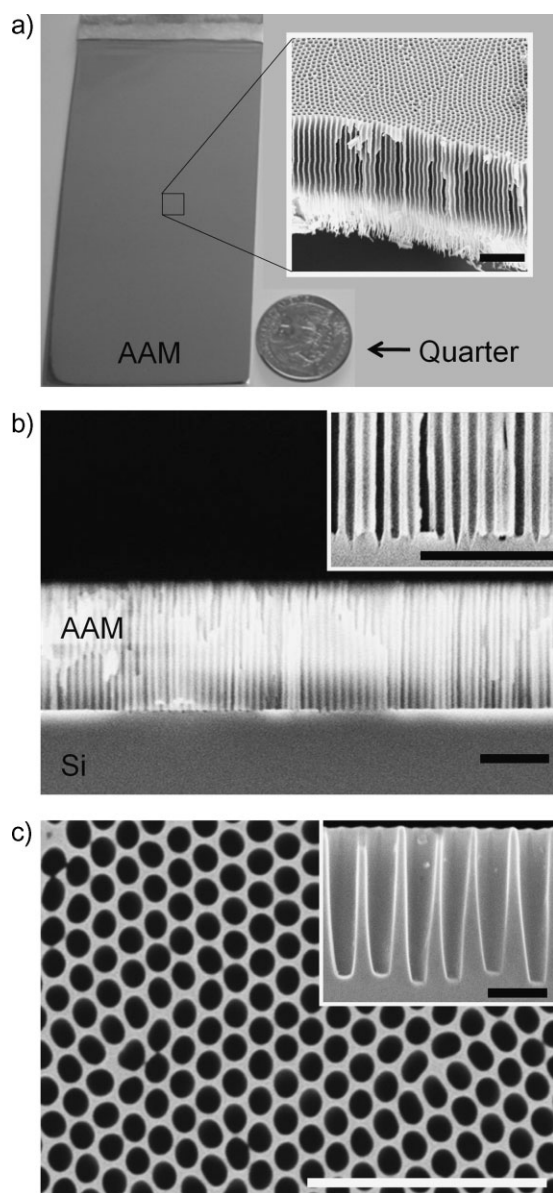


**Figure 2.** Fabrication of nanoporous Si mold by plasma etching using an anodized alumina membrane (AAM) as a mask. a) 2 inch  $\times$  4 inch AAM compared with a quarter. The inset SEM image shows the cross section of an AAM etch mask. The scale bar is 1  $\mu\text{m}$ . b) Mask-substrate assembly after removing the branches from the AAM mask. The inset is a magnified image of the mask-Si interface. The scale bars are 1  $\mu\text{m}$ . c) Si mold after the second ICP etching step. The scale bar is 1  $\mu\text{m}$ . The inset shows the cross section of the nanopores in the Si mold. The scale bar is 0.2  $\mu\text{m}$ .

(inset). When the SU-8 thickness was reduced from 200 to 145 nm, the residual layer was eliminated, resulting in discrete nanorods in solution (Figure 4b). This is simply because the mold volume depleted the SU-8 and the underlying PMMA was able to partially fill the mold, resulting in lateral separation of the SU-8 pillars. Under this condition, the nanorods had an average diameter of  $75 \pm 7$  nm at the base and a length of  $260 \pm 20$  nm. Using Si molds with a larger pore depth (e.g., 700 or 1100 nm, see Supporting Information, Figure S2), we were able to control the length of the nanorods by varying the SU-8

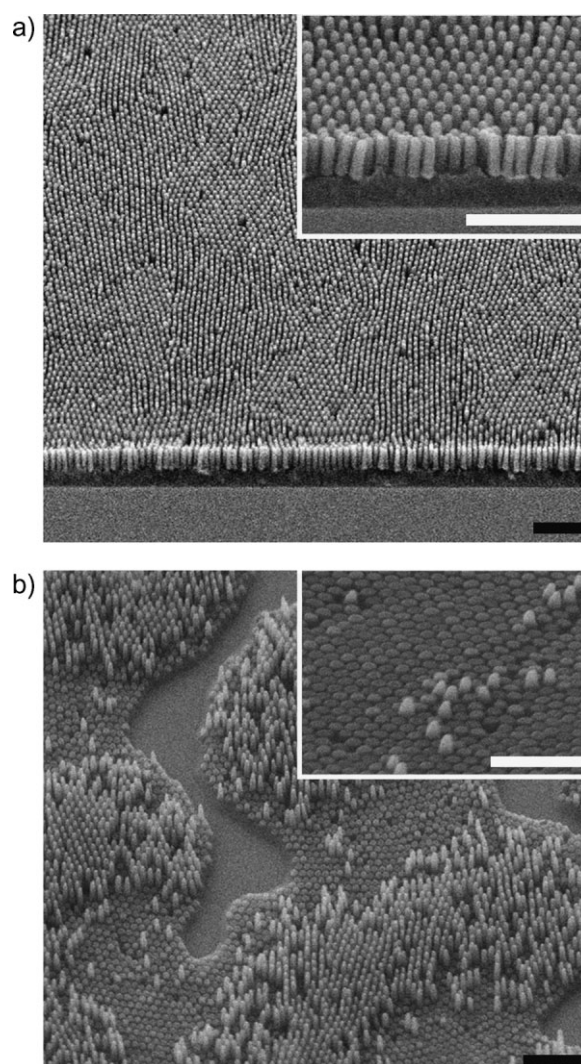


**Figure 3.** Effect of the sacrificial PMMA layer on the formation of nanopillars. a) SEM images of representative nanopillars from a bilayer substrate (SU-8 on PMMA). b) SEM images of representative nanostructures from a single-layer substrate (SU-8). The scale bars are 1  $\mu\text{m}$  in all the images.

thickness (Figure 4c). When the nanorod length was plotted against SU-8 thickness, a linear correlation with a slope of 2.2 was obtained (Figure 4c, see also Supporting Information). To demonstrate the potential for producing functional nanorods, we incorporated a fluorescent BODIPY dye into the SU-8 matrix (0.06%). A Si mold with  $\approx 1.1$ - $\mu\text{m}$ -deep pores was used to produce high-aspect-ratio fluorescent SU-8 nanoparticles of  $940 \pm 55$  nm in length and  $103 \pm 10$  nm in diameter at the base (Figure 4d). Interestingly, confocal laser scanning microscopy showed asymmetrical punctate particles that agree with the nonspherical shape of the nanorods.

In summary, this study describes a method based on nanoimprint lithography to produce uniform, free-standing, rod-shaped nanoparticles with precisely controllable dimensions. The uniqueness of the B-NIL method stems from the bilayer polymer design and development of low-cost, large-area nanoporous Si molds. The residue layer of functional polymer can be eliminated by varying the imprinting

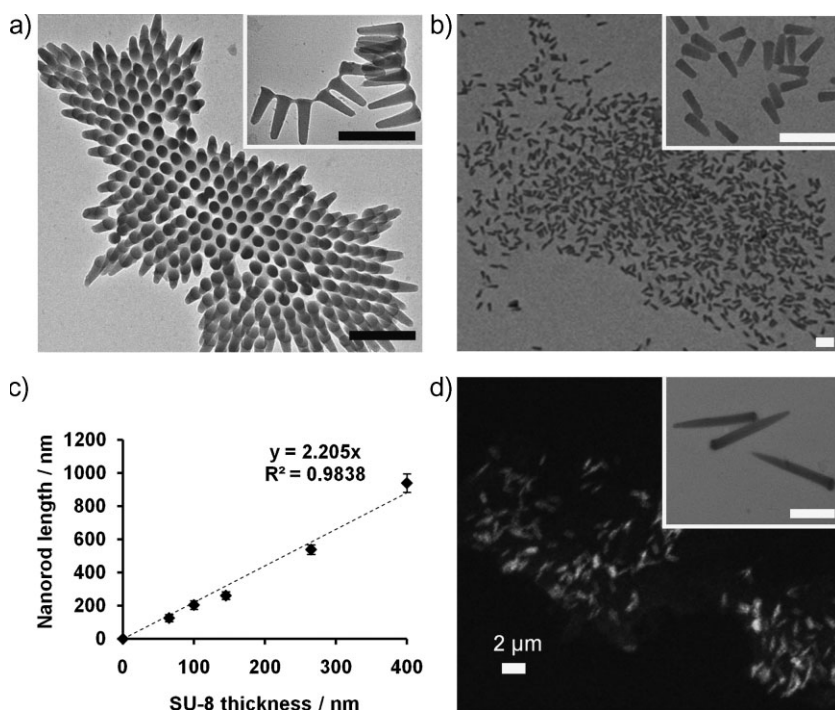


**Figure 4.** Fabricated SU-8 nanorods with tunable length. a) TEM images showing the formation of nanorods joined by a residual layer. b) TEM images of free-standing 260-nm-long nanorods. c) Nanorod length as a function of spin-coated SU-8 thickness. d) Fluorescence image of high-aspect-ratio BODIPY-doped nanorods of  $\approx 1 \mu\text{m}$  in length. The inset is a TEM image of the same particles. Scale bars are  $0.5 \mu\text{m}$  in all the TEM images.

temperature so that the bottom sacrificial polymer (higher  $T_g$ ) separates the top functional polymer nanostructures (lower  $T_g$ ) during the two-step imprinting process. The sacrificial PMMA layer enables non-invasive harvesting of nanoparticles from the substrate by dissolving the PMMA using solvents. In addition, the sacrificial layer facilitates the formation of uniform nanopillars even from an ultrathin (e.g., 65 nm) functional-polymer layer, which was not feasible with the single-layer approach. The length of these particles can be fine tuned by varying the initial polymer thickness and imprint conditions. By utilizing an AAM as an etch mask, large-area Si molds were produced with a high density of ordered nanopores. Using these molds, the B-NIL method can generate  $10^{10}$  particles per  $\text{cm}^2$  area in one imprint cycle. Compared to conventional mold fabrication techniques such as e-beam lithography, this mold production method is rapid and cost effective. Due to its parallel printing nature, similar to conventional NIL and PRINT,<sup>[20]</sup> the throughput of the B-NIL process is higher than scanning-beam or scanning-probe lithography, and microfluidic patterning. However, it is still much lower than emulsion polymerization. One promising scale-up strategy is to use roll-replication technology, such as roll-to-roll nanoimprint or embossing techniques.<sup>[39,40]</sup> In addition, the AAM transferred molds are limited to produce only cylindrical nanoparticles, although their diameter and length can be varied in a controlled manner. To print arbitrarily shaped particles using B-NIL, conventional molds defined by lithography will be required.

The availability of uniformly distributed, rod-shaped nanoparticles can provide a useful tool in various biological applications. Recent studies show that shape plays a critical role at the nanoscale in biological applications. For example, cylindrically shaped micelles persisted much longer in blood circulation,<sup>[41]</sup> and dextran-coated iron oxide “nanoworm” particles showed greater accumulation and retention at tumor sites than their spherical counterparts.<sup>[42]</sup> Conceivably, multifunctional nanorods with tunable dimensions (i.e., diameter and length) and controllable compositions (e.g., imaging agents) can be produced to study the fundamental role of particle size and geometry in biology. This, in turn, may open up opportunities for the use of nonspherical nanoparticles in molecular imaging and targeted therapeutic applications.

## Experimental Section

**Preparation of AAM etch masks:** We used a two-step anodization method followed by a voltage-reduction protocol to produce the AAM masks. Briefly, aluminum foil (99.998%) was first polished with alumina-embedded polishing pads and then ultrasonicated in acetone for 1 h. The foil was annealed at  $500^\circ\text{C}$  and subjected to electropolishing at 15 V for 30 min using a Pb cathode. The electropolishing solution was composed of 95 wt%  $\text{H}_3\text{PO}_4$ , 5 wt%  $\text{H}_2\text{SO}_4$  and  $20 \text{ g L}^{-1}$  of  $\text{CrO}_3$  and was kept at  $70^\circ\text{C}$ . The anodization steps were carried out in 5 wt% aqueous oxalic acid solution at  $8^\circ\text{C}$  under 50 V against a cylindrical stainless-steel cathode. After the first anodization, the precursor alumina film was dissolved in an aqueous solution ( $0.2 \text{ M CrO}_3$  and  $0.4 \text{ M H}_3\text{PO}_4$ ) at  $80^\circ\text{C}$ . The second anodization step took 10 min at 50 V and then the voltage was gradually decreased until the voltage was 15 V (5% decrease every 2 min). This sample was immersed in 10 wt%  $\text{H}_3\text{PO}_4$  solution for 1 h until rapid bubble formation was observed. The Al foil was carefully washed with purified water several times and AAM film was collected with a thin parafilm backing paper.

**Fabrication of nanoporous Si mold:** A Si[100] wafer was first cleaned by ultrasonication in acetone and isopropanol (15 min in each solvent) and then blown dry with nitrogen. The AAM mask was placed on top of the Si wafer with the barrier side facing up. The masked Si was etched using a two-step inductively coupled plasma (Oerlikon Versaline-ML ICP Processing System). The first etching step was a 10–12 min Ar-plasma etch (physical etch) that removes the rough branches on the barrier side. The plasma conditions were 13.56 MHz, 300 W ICP, 200 W RF bias, 10 mTorr Ar pressure, and 20 sccm Ar flow rate. The second etching step formed the ordered pores on Si through ion-enhanced etching and consisted of three etching cycles (3 min each). The pressure was 5, 10, and 15 mTorr for the three cycles. The plasma conditions

were 13.56 MHz, 300 W ICP, 200 W RF bias, and 10 sccm Ar and Cl<sub>2</sub> flow rates. Si molds with 400-nm-deep pores were formed under this condition. Keeping other variables constant, the total chemical-etching time was increased from 9 to 18 min (3 × 6 min) to obtain 700-nm-deep pores, and to 36 min (3 × 12 min) to obtain 1100-nm-deep pores in Si. The Si mold was rendered nonadhesive by immersing the mold in a solution of 1% 1H,1H,2H,2H-perfluorodecyl-trichloro silane (FOTS) in *n*-heptane for 3 min. The mold was then washed with acetone and annealed at 110 °C for 10 min. The Si mold can be reused multiple times without obvious damage. However, the FOTS coating layer degrades even after a couple of imprints<sup>[28]</sup> and repeated surface treatment is required.

**Polymer spin-coating:** A Si or quartz substrate was first spin-coated with 170-nm-thick PMMA (495 kDa) unless otherwise mentioned. The PMMA coating was baked on a hot plate at 175 °C for 10 min. Then, a layer of SU-8 was spin-coated with a thickness of 65, 100, 145, 200, 265, or 400 nm. The SU-8 film was then baked at 95 °C in an oven for 3 min. In order to prepare fluorescent particles, BODIPY FL dye was dissolved in the SU-8 matrix at a weight percentage of 0.06%. The polymer film thickness was measured using a Veeco Dektak VIII Profilometer.

**Nanoimprinting and particle harvesting:** The polymer-coated substrate was brought into contact with the FOTS-treated Si mold. This assembly was heated to 100 °C under 4 MPa (Obducat Nanoimprinter 2.5) for the SU-8 flow. The temperature was then ramped up to 170 °C to allow the flow of PMMA. After 10 min, the imprinter system was cooled down to room temperature and the mold was released from the substrate. The imprinted SU-8 structures were then crosslinked using UV radiation ( $\lambda_{\text{max}} = 365 \text{ nm}$ ,  $10 \text{ mW cm}^{-2}$ ) for 30 to 60 s and further baked at 95 °C to minimize stress. Then, the sample was soaked in acetone with ultrasonic agitation for a few minutes. The solution containing the SU-8 nanorods and dissolved PMMA was centrifuged at 2000–7000 rpm and the supernatant containing PMMA was removed. Nanorods were collected and further washed by acetone and water (see the Supporting Information for details on particle characterization). Note that the SU-8 nanostructures are referred to as nanopillars if they are bound to the surface, and as nanorods after they are liberated into solution.

## Keywords:

anodic alumina membranes · fluorescent nanorods · nanoimprint lithography · nanoporous silicon · nonspherical nanoparticles

- [1] M. Ferrari, *Nat. Rev. Cancer* **2005**, *5*, 161.  
 [2] D. Peer, J. M. Karp, S. Hong, O. C. Farokhzad, R. Margalit, R. Langer, *Nat. Nanotechnol.* **2007**, *2*, 751.  
 [3] L. E. Euliss, J. A. DuPont, S. Gratton, J. DeSimone, *Chem. Soc. Rev.* **2006**, *35*, 1095.  
 [4] J. A. Champion, Y. K. Katere, S. Mitragotri, *Proc. Natl. Acad. Sci. USA* **2007**, *104*, 11901.  
 [5] U. S. Tandon, *Vacuum* **1992**, *43*, 241.  
 [6] S. Y. Chou, P. R. Krauss, P. J. Renstrom, *Science* **1996**, *272*, 85.  
 [7] P. Ruchhoeft, M. Colburn, B. Choi, H. Nounu, S. Johnson, T. Bailey, S. Damle, M. Stewart, J. Ekerdt, S. V. Sreenivasan, J. C. Wolfe, C. G. Willson, *J. Vac. Sci. Technol. B* **1999**, *17*, 2965.  
 [8] Y. N. Xia, G. M. Whitesides, *Annu. Rev. Mater. Sci.* **1998**, *28*, 153.

- [9] R. D. Piner, J. Zhu, F. Xu, S. H. Hong, C. A. Mirkin, *Science* **1999**, *283*, 661.  
 [10] R. J. Jackman, J. L. Wilbur, G. M. Whitesides, *Science* **1995**, *269*, 664.  
 [11] J. C. Love, K. E. Paul, G. M. Whitesides, *Adv. Mater.* **2001**, *13*, 604.  
 [12] M. Geissler, J. M. McLellan, Y. N. Xia, *Nano Lett.* **2005**, *5*, 31.  
 [13] C. M. Bruinink, M. Peter, P. A. Maury, M. De Boer, L. Kuipers, J. Huskens, D. N. Reinhoudt, *Adv. Func. Mater.* **2006**, *16*, 1555.  
 [14] J. Zaumseil, M. A. Meitl, J. W. P. Hsu, B. R. Acharya, K. W. Baldwin, Y. L. Loo, J. A. Rogers, *Nano Lett.* **2003**, *3*, 1223.  
 [15] S. Y. Chou, L. Zhuang, *J. Vac. Sci. Technol. B* **1999**, *17*, 3197.  
 [16] J. E. Meiring, M. J. Schmid, S. M. Grayson, B. M. Rathasack, D. M. Johnson, R. Kirby, R. Kannappan, K. Manthiram, B. Hsia, Z. L. Hogan, A. D. Ellington, M. V. Pishko, C. G. Willson, *Chem. Mater.* **2004**, *16*, 5574.  
 [17] D. Dendukuri, D. C. Pregibon, J. Collins, T. A. Hatton, P. S. Doyle, *Nat. Mater.* **2006**, *5*, 365.  
 [18] D. Dendukuri, K. Tsoi, T. A. Hatton, P. S. Doyle, *Langmuir* **2005**, *21*, 2113.  
 [19] S. Xu, Z. Nie, M. Seo, P. Lewis, E. Kumacheva, H. A. Stone, P. Garstecki, D. B. Weibel, I. Gitlin, G. M. Whitesides, *Angew. Chem. Int. Ed.* **2005**, *44*, 724.  
 [20] J. P. Rolland, B. W. Maynor, L. E. Euliss, A. E. Exner, G. M. Denison, J. M. DeSimone, *J. Am. Chem. Soc.* **2005**, *127*, 10096.  
 [21] L. C. Glangchai, M. Caldorera-Moore, L. Shi, K. Roy, *J. Controlled Release* **2008**, *125*, 263.  
 [22] C. C. Ho, A. Keller, J. A. Odell, R. H. Ottewill, *Coll. Polym. Sci.* **1993**, *271*, 469.  
 [23] Y. Lu, Y. Yin, Y. Xia, *Adv. Mater.* **2001**, *13*, 271.  
 [24] S. E. A. Gratton, P. D. Pohlhaus, J. Lee, J. Guo, M. J. Cho, J. M. DeSimone, *J. Controlled Release* **2007**, *121*, 10.  
 [25] H. Masuda, K. Fukuda, *Science* **1995**, *268*, 1466.  
 [26] R. S. Shawgo, A. C. R. Grayson, Y. W. Li, M. J. Cima, *Curr. Opin. Solid State Mater. Sci.* **2002**, *6*, 329.  
 [27] F. Walther, P. Davydovskaya, S. Zucher, M. Kaiser, H. Herberg, A. M. Gigler, R. W. Stark, *J. Micromech. Microeng.* **2007**, *17*, 524.  
 [28] L. Tao, S. Ramachandran, C. T. Nelson, M. Lin, L. J. Overzet, M. Goeckner, G. Lee, C. G. Willson, W. Wu, W. Hu, *Nanotechnology* **2008**, *19*.  
 [29] S. Y. Chou, P. R. Krauss, P. J. Renstrom, *Appl. Phys. Lett.* **1995**, *67*, 3114.  
 [30] M. C. Kang, S. F. Yu, N. C. Li, C. R. Martin, *Langmuir* **2005**, *21*, 8429.  
 [31] Y. Li, Y. Kanamori, K. Hane, *Microsyst. Technol.* **2004**, *10*, 272.  
 [32] J. Y. Liang, H. L. Luo, R. Beresford, J. Xu, *Appl. Phys. Lett.* **2004**, *85*, 5974.  
 [33] H. Masuda, A. Abe, M. Nakao, A. Yokoo, T. Tamamura, K. Nishio, *Adv. Mater.* **2003**, *15*, 161.  
 [34] Y. D. Wang, S. J. Chua, M. S. Sander, P. Chen, S. Tripathy, C. G. Fonstad, *Appl. Phys. Lett.* **2004**, *85*, 816.  
 [35] N. Li, D. T. Mitchell, K.-P. Lee, C. R. Martin, *J. Electrochem. Soc.* **2003**, *150*, A979.  
 [36] R. C. Furneaux, W. R. Rigby, A. P. Davidson, *Nature* **1989**, *337*, 147.  
 [37] S. Landis, N. Chaix, D. Hermelin, T. Leveder, C. Gourgon, *Microelectron. Eng.* **2007**, *84*, 940.  
 [38] C. L. Soles, E. K. Lin, J. L. Lenhart, R. L. Jones, W.-I. Wu, D. L. Goldfarb, M. Angelopoulos, *J. Vac. Sci. Technol. B* **2001**, *19*, 2690.  
 [39] S. Ahn, J. Cha, H. Myung, S.-m. Kim, S. Kanga, *Appl. Phys. Lett.* **2006**, *89*.  
 [40] S. H. Ahn, L. J. Guo, *Adv. Mater.* **2008**, *20*.  
 [41] Y. Geng, P. Dalhaimer, S. S. Cai, R. Tsai, M. Tewari, T. Minko, D. E. Discher, *Nat. Nanotechnol.* **2007**, *2*, 249.  
 [42] J. H. Park, G. von Maltzahn, L. L. Zhang, M. P. Schwartz, E. Ruoslahti, S. N. Bhatia, M. J. Sailor, *Adv. Mater.* **2008**, *20*, 1630.

Received: December 6, 2008  
 Revised: February 22, 2009  
 Published online: